NANO LETTERS

2007
Vol. 7, No. 2
300−306

Extrinsic and Intrinsic Effects on the Excited-State Kinetics of Single-Walled Carbon Nanotubes

Marcus Jones,[†] Wyatt K. Metzger,[§] Timothy J. McDonald,[‡] Chaiwat Engtrakul,[‡] Randy J. Ellingson,[†] Garry Rumbles,*[,†] and Michael J. Heben*[,‡]

National Renewable Energy Laboratory, Golden, Colorado 80401-3393

Received September 27, 2006; Revised Manuscript Received January 8, 2007

ABSTRACT

We characterized the photoluminescence (PL) decay of 15 different, solubilized single-walled carbon nanotubes with tube diameters that ranged from 0.7 to 1.1 nm using time-correlated single photon counting. Each nanotube species was excited resonantly at the second excited state, E_2, and PL was detected at the lowest energy exciton emission, E_1. In a 10 ns window, the PL decays were described well by a biexponential fitting function with two characteristic time constants, suggesting that at least two kinetically distinct relaxation processes were observed. The dominant decay component increased from 60 to 200 ps with increasing tube diameter, while the lesser component, which contributed up to 8% of the total decay, increased from 200 ps to 4.8 ns. The observation of the second, longer decay time component is examined in terms of two possible models: an extrinsic behavior that implicates sample inhomogeneity and an intrinsic process associated with interconversion between kinetically distinct bright and dark exciton states. A common conclusion from both models is that nonradiative decay controls the PL decay by a process that is diameter dependent.

Since their discovery, single-walled carbon nanotubes (SWNTs) have been intensely investigated from a variety of perspectives. From an optoelectronics point of view, it is striking that different nanotube species have distinct metallic and semiconducting character based upon their structure. Understanding of the relaxation mechanisms after optical excitation has been hindered by the fact that tubes exist and interact in bundles in which tube types and characters are mixed. As a result, it was not until 2002 that near-infrared photoluminescence (PL) was detected after SWNT bundles were disrupted and isolated tubes were produced in surfactant solutions.[1] Studies performed on solutions of dispersed SWNTs have significantly expanded the understanding of photoexcitation relaxation processes. For example, there is now experimental evidence that photoexcitation of semiconducting nanotubes generates excitons that may be described by calculations that incorporate electron−electron interactions.[2−9] A detailed understanding of these issues will aid in the deployment of SWNTs in a variety of important applications such as those that relate to the conversion of solar energy.

One of the first transient luminescence experiments used the fluorescence upconversion technique and observed fast (100 fs) PL decay (τ_{PL}) due to exciton−exciton annihilation at high pump fluences.[10] Time-correlated single photon counting (TCSPC) and a Kerr gating technique were used to measured τ_{PL} of 15[11] and 7 ps,[12] respectively, for tube populations that were excited off-resonance at a fixed wavelength. A distribution of relaxation times was noted and attributed to dispersity in nanotube type and length or the presence of structural imperfections. Using TCSPC, Reich et al. measured τ_{PL} for five different nanotubes and determined values in the range 25 ± 5 ps with no obvious dependence upon diameter.[13] We also previously employed TCSPC and measured one of the longest τ_{PL} values reported to date of 130 ± 10 ps for three nanotubes species, all of which were of similar diameter. Interestingly, we found a small component of the PL yield (1%) that was much slower, with a time constant in the range of 1.5 to 1.7 ns, a value that was also seen in the transient bleach data from the same samples.[14] There have been a number of reports using other excited-state spectroscopies, such as transient absorption[3,10,13,15−18] and transient grating[5] experiments, where a range of excited-state lifetimes and processes have been reported, but like the PL studies, there are inconsistencies in the magnitude of the excited-state lifetime. Exciton−exciton annihilation, caused by high laser fluences is likely present in several of these studies, and the presence of both bundled and isolated nanotubes complicates the picture. In short, despite a substantial amount of work, the photoexcitation relaxation mechanisms in SWNTs are still not well understood. The

* Corresponding authors. E-mail: michael_heben@nrel.gov (M.J.H.); garry_rumbles@nrel.gov (G.R.).
[†] Chemical and Biosciences Center.
[‡] Materials Science Center.
[§] National Center for Photovoltaics.

10.1021/nl0622808 CCC: $37.00
Published on Web 01/23/2007

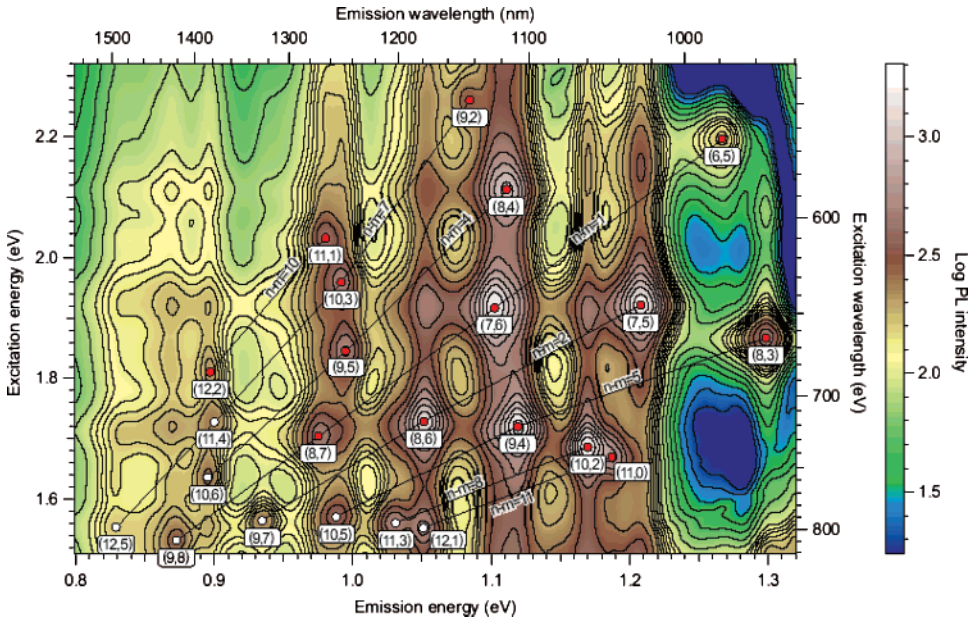

Figure 1. Room-temperature PL contour map of the SDBS/SWNT sample in water. The data are plotted with intensity in logarithmic form so as to enhance the weaker peaks at low emission energies. A total of 23 separate semiconducting SWNT species are identified, and time-resolved PL was recorded for each of the tubes marked with red dots.

range in reported τ_{PL} values is likely due to the fact that time windows, excitation levels and energies, and the samples themselves vary from lab to lab.

The range in the photoluminescence lifetimes, τ_{PL}, has led to a similar range for the natural radiative lifetime, τ_R, which has been reported as 110 ns, 260 ns, or even 3.2 μs.[12,19,20] Interestingly, none of these values agree well with recent calculations for τ_R, which span from 2 to 4 ns, or 30 to 40 ns, depending on whether there is thermalization within the singlet exciton manifold alone or if mixed singlet−triplet manifolds are involved.[21] It is important to note that such calculations account only for intrinsic characteristics associated with the position in energy of the photoexcited states and do not address extrinsic factors such as impurities, defects, tube−tube and tube-substrate interactions, and/or finite length effects. The fact that extrinsic factors play a key role is underscored by the observation that τ_{PL} values for the same (6,4) nanotube varied from 20 to 180 ps, as different individual species were probed.[22] Thus, in general, there are two approaches to understanding the photoexcitation relaxation dynamics in SWNTs, one of which considers the redistribution of energy within excited-state manifolds, and a second which considers the photophysics to be dominated by extrinsic factors.

In this article, we report on the PL decay from 15 different solubilized SWNTs that span a diameter range from 0.7 to 1.1 nm and emit over a wide spectral window. Each tube type was resonantly excited at the E_2 transition and detected at the lowest exciton emission energy, E_1. We found it necessary to employ a biexponential function to accurately fit the data, indicating that at least two kinetically distinct species can be observed. We investigate the application of an intrinsic model, where interconversion between kinetically distinct bright and dark exciton states is considered, and an extrinsic model, where sample heterogeneities are assumed to govern the nanotube PL kinetics. Both models find that nonradiative processes control the PL decay by a process that is diameter dependent.

Following the procedure of previous reports,[1] 12 mg of as-produced HiPco SWNTs (Carbon Nanotechnologies) were suspended in 15 mL of aq sodium dodecylbenzene sulfonate (SDBS) surfactant (1 wt %) using a cup-horn sonicator driven by an ultrasonic processor (Cole-Palmer, 750 W). The mixture was kept in a water bath cooled to 15 °C during the sonication period (12 min). The resulting suspension was centrifuged (Beckman Coulter, Optima XL-100K) at 104 000 g for 4 h using a swing bucket rotor (SW-28). A stable suspension of SWNTs was isolated by decanting the upper 75% of the supernatant, which was used in subsequent experiments.

Photoluminescence excitation (PLE) and emission (PL) contour maps were obtained with a modified Thermo-Electron FT960 Raman system that contains a Ge detector operating at 77 K that responds to wavelengths between 900 and 1700 nm. The excitation source, a 250 W tungsten halogen bulb coupled to a single-grating monochromator, produces monochromatic light between 400 and 1100 nm with a peak power of 1.7 mW at 700 nm. All spectra were corrected for intensity variations in the lamp spectrum as well as for the response of the FT system and detector.[23] The steady-state PL spectral contour map of the SWNT sample is presented in Figure 1 with (n,m) assignments based on the work of Weisman et al.[1,24]

Transient, photoluminescence decay curves were measured at ambient temperatures using time-correlated single-photon counting (TCSPC),[25] recording data in the range of 5000−10 000 counts in the channel of maximum intensity, depending upon the relative intensity of the SWNT PL. Photoexcitation was provided by an optical parametric amplifier pumped by the output of a titanium:sapphire laser system

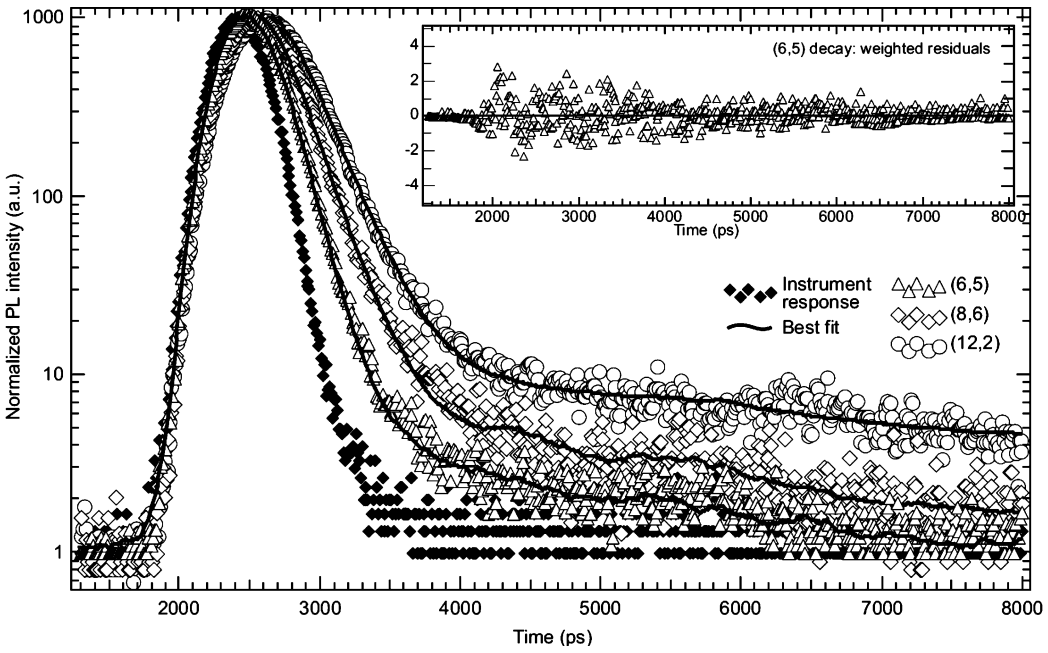

Figure 2. Representative PL transients from three tube species: (6,5) triangles, (8,6) diamonds, and (12,2) circles, having diameters of 0.76, 0.97, and 1.04 nm, respectively. The instrument response used in fitting the (6,5) decay is represented by black diamonds, and the thick black lines are the best-fit decay curves. The inset shows a plot of weighted residuals for the fit to the data for the (6,5) nanotube.

with a regenerative amplifier. The desired wavelength was chosen to match the second exciton absorption peak (E_2), which was determined from the steady-state PL contour map (Figure 1). The final laser output consisted of a 250 kHz pulse train with a pulse width of several hundred femtoseconds and a spot size 3.5 mm in diameter. The measurements were performed with approximately 20 nJ per pulse for all tubes, with the exception of the (12,2) species, which required 80 nJ per pulse. Cuvettes with 3 mm entry and exit windows were used, and PL from the SWNT solutions was detected perpendicular to the excitation beam to mitigate the amount of scattered light incident on the detector. The PL was passed through long pass filters, a spectrometer, and was subsequently detected by a cooled (80 K) infrared-sensitive photomultiplier tube (Hamamatsu R5509). Instrument response functions (IRFs) were measured, detecting scattered excitation light from the same samples as those from which fluorescence was viewed. Time-resolved PL transients were recorded for all of the tubes labeled in Figure 1.

PL decay curves were analyzed by nonlinear least-squares iterative reconvolution of a model sum-of-exponentials decay function with the measured instrument response functions.[25] This technique removes the contribution of the IRF to the measured decay, resulting in a temporal resolution of ~40 ps, which is approximately 10% of the full width at half-maximum intensity of the measured instrument response function.[25] Because of the high signal-to-noise ratio of TCSPC data, stringent statistical analyses of the fit of the decay function to the experimental data could be employed to judge the goodness of fit. These included: a random distribution plot of weighted residuals, a reduced chi square close to 1.0, and a serial correlation coefficient of ~1.7. The validity of this approach was verified by measuring PL decays from a dilute solution of a reference dye (IR26) that absorbed and emitted with a wavelength-independent decay profile in the same spectral window as the SWNT samples.[18,26]

Representative, PL transients (normalized) recorded in a 10 ns window for three SWNT species, (6,5), (8,6), and (12,2), are presented in Figure 2. Each of the three PL response curves are characterized by a dominant initial decay followed by a slower process, which, taken together, can be well-fit using a double exponential decay function of the form:

$$I(t) = A_1 \exp(-t/\tau_1) + A_2 \exp(-t/\tau_2) \qquad (1)$$

The parameters derived from these and 12 additional SWNTs (identified by the red dots in Figure 1) are presented in Table 1, along with the fractional yield, Y_n, that each decay time component, τ_n, contributes to the PL decay profile from each SWNT, as determined by:

$$Y_n = \frac{A_n \tau_n}{\sum_i A_i \tau_i} \times 100\% \qquad (2)$$

The short decay time component, τ_1, has values that range smoothly from ~60 ps for narrow diameter tubes to ~200 ps for larger diameter tubes. Although the τ_2 components are readily observed and necessary to achieve a good fit to the data, the τ_1 components contribute between 97% and 99% of the integrated PL decay for the majority of the tube species and ~100% in the cases of the (11,0) and (9,4) tubes (Table 1). The contribution of the τ_2 component is more substantial for the (8,7), (8,3), and (12,2) species and increases in both magnitude and yield with increasing tube diameter, as can

Table 1. Photoluminescence Decay Times (τ_1 and τ_2) Recorded for 15 Specific Nanotubes of Indices (n,m) Measured at the Optical Band Edge, E_1, and Assigned According to Weisman et al.[24] [a]

SWNT species				decay time component 1			decay time component 2		
n	m	diameter/nm	E_1/eV	A_1	τ_1/ps	yield$_1$/%	A_1	τ_2/ps	yield$_2$/%
6	5	0.757	1.268	0.998	113	98.4	0.002	957	1.6
8	3	0.782	1.299	0.969	63	91.1	0.031	194	8.9
9	2	0.806	1.083	0.997	142	98	0.003	1024	2
7	5	0.829	1.209	0.992	95	96.9	0.008	380	3.1
8	4	0.84	1.111	0.999	124	98.9	0.001	1425	1.1
11	0	0.873	1.187	1	125	100			
10	2	0.884	1.169	0.998	120	98.8	0.002	662	1.2
7	6	0.895	1.102	0.997	110	98.6	0.003	616	1.4
9	4	0.916	1.119	1	131	100			
11	1	0.916	0.981	0.997	155	97.2	0.003	1642	2.8
10	3	0.936	0.992	0.997	152	97.1	0.003	1403	2.9
8	6	0.966	1.052	0.999	152	98	0.001	2829	2
9	5	0.976	0.995	0.998	167	97.2	0.002	2123	2.8
8	7	1.032	0.976	0.997	173	94.1	0.003	4006	5.9
12	2	1.041	0.897	0.996	206	92.1	0.004	4848	7.9

[a] Yields are calculated using eq 2.

be seen from the three decay profiles displayed in Figure 2. The only clear exception is the (8,3) tube, which has a much larger (8.9%) τ_2 component than tubes of similar diameter.

Three important conclusions arise from these data: First, the PL decay profile cannot be adequately described by a single-exponential decay function, with a characteristic PL lifetime, but requires a biexponential function with two characteristic decay times. Second, the dominant of these two characteristic decay times increases from 60 ps to 200 ps with decreasing emission energy, indicating a correlation with tube diameter. Third, the presence of a second, longer decay time necessitates the use of a kinetic model having more than one kinetically distinct process.

The dominant decay time component observed for the narrowest diameter nanotubes is ~100 ps, a value similar to that reported in our previous study[22] of isolated SWNTs nanotubes emitting in the same, narrow, spectral region, and also observed in on-resonance transient absorption measurements.[18] The present extension of the study to lower energy, where larger diameter nanotubes emit, reveals a systematic increase in this decay time to 200 ps. The consistency with which we repeatedly extract similar values for the dominant, shortest decay time, with the 15 different SWNTs reported here, and with a different surfactant, have confirmed the reproducibility of our sample preparation. The absence of a short component (~10 ps), which has been reported by others,[10,12] could be due to sample preparations being different in different labs, or perhaps be ascribed to the high laser powers associated with, for example, the frequency upconversion technique. High laser powers have been shown to cause significant exciton−exciton annihilation, resulting in a fast decay in the PL signals at early times.[3,9,16] Attempts to mimic these conditions in our TCSPC experiment did not result in any noticeable appearance of a fast decay, although the highest pump fluences that we could achieve were still an order of magnitude or two less than these studies. To address the possibility that a dominant, fast component could go unnoticed in the TCSPC experiment, we simulated the data using two different approaches.[25,27] Both exercises demonstrated that any short-lived components must exist at relative yields less than 10%.

The two characteristic decay times from Table 1 are plotted against nanotube diameter in Figure 3. To explain these trends, it is necessary to first identify a kinetic scheme whose solution predicts a biexponential decay function with two characteristic decay times. The most general scheme of this type has two interacting species, A* and B*, which decay either radiatively or nonradiatively such that the time dependence of both species decays according to the general function:

$$i(t) = A_1 \exp(-\lambda_1 t) + A_2 \exp(-\lambda_2 t) \qquad (3)$$

where λ_1 and λ_2 are the solutions to the two simultaneous, first-order differential equations and are the inverse of the two measured decay times, τ_1 and τ_2. The general scheme and a detailed solution are provided in the Supporting Information.

The two characteristic rate coefficients derived from the simultaneous differential equations are, in general, independent of whether A* or B* is excited and also independent of whether emission is detected from A* or B*. In all cases, it is only the pre-exponential factors that are affected. Using this basic scheme, two specific cases are considered that are both consistent with the data, but adopt different assumptions. The first is based on extrinsic effects due to heterogeneities in the sample, the second on intrinsic effects caused by interconverting excitonic states within a single nanotube species.

1. Extrinsic Model. In this scenario, A* and B* represent two excited-state nanotube species of the same (n,m) type that may differ in, for example, length, defect density, and interactions with neighbors. These two species are populated indirectly via internal conversion of the initially excited exciton states and emit at the same wavelength, but with no

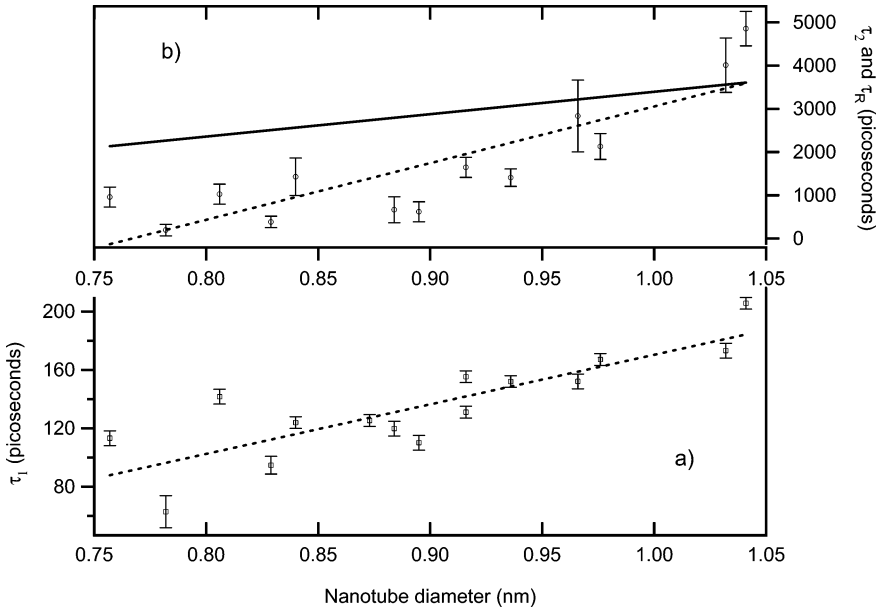

Figure 3. Plot of decay times for (a) τ_1 and (b) τ_2 against nanotube diameter for the 15 SWNT species, with dotted lines provided as a guide to the eye. The solid line in (b) corresponds to the theoretical prediction of the natural radiative lifetime, τ_R, for these SWNTs.[21]

Scheme 1. Kinetic Scheme to Describe the Origin of the Biexponential Decay Behavior Associated with the Extrinsic Model

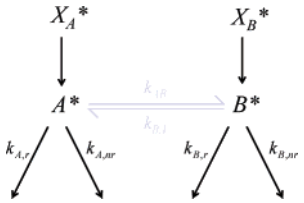

exchange of excitation energy, such that the kinetic scheme reduces to Scheme 1.

With no interconversion between A* and B*, the two decay times from eq 3 become:

$$(\tau_1)^{-1} = \lambda_1 = k_A = k_{A,r} + k_{A,nr} \quad (4)$$

$$(\tau_2)^{-1} = \lambda_2 = k_B = k_{B,r} + k_{B,nr} \quad (5)$$

such that τ_1 and τ_2 now represent the PL lifetimes of species A* and B*, respectively. The radiative rate constants $k_{A,r}$ and $k_{B,r}$ are considered equal, and therefore, the difference between the slow and fast lifetimes occurs as a result of different nonradiative decay constants. In this scenario, the yields quoted in Table 1 represent the amount of PL contributed to the integrated intensity by the two species, and with an estimate of the natural radiative lifetimes, $\tau_{A,r} = (k_{A,r})^{-1}$ (or $\tau_{B,r} = (k_{B,r})^{-1}$), such as those provided by Perebeinos et al.,[21] it is possible to relate these to the photoluminescence quantum yield (PLQY) for each type of tube species. Furthermore, with singlet excitons contributing to the radiative process, the predicted values of the natural radiative lifetime increase with increasing nanotube diameter, in a similar fashion to the measured PL lifetimes, as shown in Figure 3. For nanotube species with the fast PL lifetime (species A*), these natural radiative lifetimes are significantly longer than those measured, indicating that nonradiative decay dominates this measured PL lifetime. For nanotubes with a long PL lifetime (species B*), the calculated and measured values are similar, which suggests that the radiative process is the dominant decay mechanism and these nanotubes exhibit a PLQY close to unity. On the basis of this analysis, nanotube species A* and B* are distinguished through differing amounts, or efficiency, of quenching traps created during growth, purification, or preparation of surfactant-stabilized solutions. Ill-defined end groups, side-wall defects, and other growth defects could also contribute to the quenching mechanism. It is also possible that small bundles of nanotubes that do not contain any metallic species could be responsible for the emission from A*, where nanotube interactions result in an efficient nonradiative decay process, while emission from B* emanates from truly isolated nanotubes. This model is similar to that proposed for TCSPC data of isolated SWNTs embedded in surfactant and deposited on a glass substrate,[22] with differing PL lifetimes observed for SWNT species of the same (*n*,*m*) indices. Extrapolation of this idea to the ensemble measurements reported here suggests that a distribution of lifetimes could be an appropriate data analysis procedure, although the signal-to-noise ratio of the data is too low to warrant such an approach. The fact that two PL decay times are extracted suggests that there is possibly a bimodal distribution of two emissive SWNT types within the extrinsic model.

Calculations of the natural radiative lifetimes that assume the singlet and triplet exciton states are equilibrated[21] can be used to estimate the individual PLQY of each nanotube species in a similar fashion with the values being an order of magnitude less than those involving singlet excitons only, a value that agrees well with recent single SWNT studies by Lefebvre et al.[28] We note that, although there are no intrinsic mechanisms for promoting intersystem crossing in

Scheme 2. Kinetic Scheme to Describe the Origin of the Biexponential Decay Behavior Associated with the Intrinsic Model

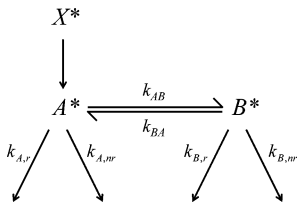

this model, the same extrinsic factors used to explain the difference between the tube species A and B might also provide a means of coupling the singlet and triplet states.

2. Intrinsic Model. Here, A* and B* represent two excitonic states, a bright state, A*, which sits energetically just above a dark state, B*. A* is populated via efficient internal conversion of the initial photoexcited excitonic state (X*) and then interacts with exciton state, B*. This concept fits well with recent theoretical and experimental studies on this subject.[3,6,8,21] Under this scenario, the kinetics are described by Scheme 2, and the two decay times remain related to the individual rate constants according to:

$$\lambda_{1,2} = \frac{1}{2}[(k_A + k_{AB} + k_B + k_{BA}) \pm \sqrt{(k_B + k_{BA} - k_A - k_{AB})^2 + 4k_{BA}k_{AB}}] = (\tau_{1,2})^{-1} \quad (6)$$

(Note: As in eqs 4 and 5, $k_A = k_{A,r} + k_{A,nr}$ and $k_B = k_{B,r} + k_{B,nr}$.)

Here τ_1 and τ_2 remain as decay times and do *not* represent the PL lifetimes of the bright and dark exciton states, although, depending upon the relative magnitude of the 6 constituent rate constants, a loose association may be made. Equally, the association of the percentage yields, Y_n, in Table 1 with the PLQY of the bright and dark excitons should not be made. For the specific condition that $k_{BA} = 0$, both of these constraints are relaxed; however, in the experiments reported here, only emission from species A* (the bright exciton) is assumed to be detected, and the fact that the longer decay time component is observed verifies that $k_{BA} \neq 0$ such that the long-lived emission is a form of delayed luminescence.

A distinct feature of the intrinsic model is the apparent kinetic isolation of the two exciton states, which, using recent calculations,[21] are significantly close in energy such that thermalization should occur and a Boltzmann distribution obtained. This is the hypothesis used to derive the natural radiative lifetimes quoted for the extrinsic model earlier; however, this model predicts that the PL decay must be monoexponential, in contrast with what is observed experimentally. Here, the increase in the decay times, τ_1 and τ_2, with increasing nanotube diameter could be simply explained in terms of a reduction in the respective nonradiative decay constants, $k_{A,nr}$ and $k_{B,nr}$, although changes in the rate constants for interconversion, k_{AB} and k_{BA}, offer additional degrees of freedom.

In summary: Using time-correlated single-photon counting, we have measured PL decay profiles within the first 10 nanoseconds after excitation for a number of solubilized SWNTs whose diameters extend over a wider range than previously reported. The decay profiles cannot be described well by a single PL lifetime but require a biexponential function with two characteristic decay time components. The shorter and dominant component is seen to increase from 60 up to 200 ps with increasing nanotube diameter. The new and longer component, however, not only increases from 0.2 to 4.8 ns over the same nanotube diameter range but also exhibits a significant increase in contribution to the PL decay for the larger diameter tubes. The need for a biexponential decay function and two characteristic decay times indicates that there are at least two, kinetically distinct species that contribute to the PL decay process in this time window. A kinetic scheme is proposed that is consistent with this new observation, and we compare two models that represent extreme cases of this general scheme. Both models offer reasons for the low photoluminescence quantum yields that are observed for isolated SWNTs, and both indicate clearly that nonradiative decay is the dominant deactivation pathway responsible for these low yields. The extrinsic model suggests that nanotube interactions or quenching at defects might be the cause of the nonradiative decay for the dominant nanotubes in the sample, with the long decay time attributed to specific, and mainly larger diameter, tubes that are more isolated. An alternative model associates the two decay times with conversion between a dark exciton that sits energetically below the bright, emissive exciton that are both intrinsic to all of the emitting nanotubes. In this scenario, the combined effects of nonradiative decay of the dark exciton state and the strength of coupling to the bright exciton are dependent on nanotube diameter, and both control the PL quantum yield and importance of the two decay times. Future improvements in sample preparation will permit more thorough testing of these two models.

Acknowledgment. This work was funded by the Photochemistry and Radiation Research program of the U.S. Department of Energy, Office of Science, Basic Energy Sciences, Division of Chemical Sciences, Geosciences and Biosciences, under contract no. DE-AC36-99GO10337 to NREL.

Supporting Information Available: Mathematical derivation of the general kinetic scheme from which Schemes 1 and 2 are derived. This material is available free of charge via the Internet at http://pubs.acs.org.

References

(1) O'Connell, M. J.; Bachilo, S. M.; Huffman, C. B.; Moore, V. C.; Strano, M. S.; Haroz, E. H.; Rialon, K. L.; Boul, P. J.; Noon, W. H.; Kittrell, C.; Ma, J. P.; Hauge, R. H.; Weisman, R. B.; Smalley, R. E. *Science* **2002**, *297*, 593−596.
(2) Ando, T. *J. Phys. Soc. Jpn.* **1997**, *66*, 1066−1073.
(3) Ma, J. P.; Spataru, C. D.; Valkunas, L.; Louie, S. G.; Fleming, G. R. *Phys. Rev. B* **2006**, *74*, 085402.
(4) Pedersen, T. G. *Carbon* **2004**, *42*, 1007.
(5) Seferyan, H. Y.; Nasr, M. B.; Senekerimyan, V.; Zadoyan, R.; Collins, P.; Apkarian, V. A. *Nano Lett.* **2006**, *6*, 1757.
(6) Spataru, C. D.; Ismail-Beigi, S.; Benedict, L. X.; Louie, S. G. *Appl. Phys. A: Mater. Sci. Process.* **2004**, *78*, 1129.

(7) Wang, F.; Dukovic, G.; Brus, L. E.; Heinz, T. F. *Science* **2005**, *308*, 838.
(8) Zhao, H. B.; Mazumdar, S. *Phys. Rev. Lett.* **2004**, *93*, 157402.
(9) Huang, L. B.; Krauss, T. D. *Phys. Rev. Lett.* **2006**, *96*, 057407.
(10) Ma, Y. Z.; Stenger, J.; Zimmermann, J.; Bachilo, S. M.; Smalley, R. E.; Weisman, R. B.; Fleming, G. R. *J. Chem. Phys.* **2004**, *120*, 3368.
(11) Hagen, A.; Moos, G.; Talalaev, V.; Hertel, T. *Appl. Phys. A: Mater. Sci. Process.* **2004**, *78*, 1137.
(12) Wang, F.; Dukovic, G.; Brus, L. E.; Heinz, T. F. *Phys. Rev. Lett.* **2004**, *92*, 177401.
(13) Reich, S.; Dworzak, M.; Hoffmann, A.; Thomsen, C.; Strano, M. S. *Phys. Rev. B* **2005**, *71*, 033402.
(14) Ellingson, R. J.; Engtrakul, C.; Jones, M.; Samec, M.; Rumbles, G.; Nozik, A. J.; Heben, M. J. *Phys. Rev. B* **2005**, *71*, 115444.
(15) Ma, Y. Z.; Valkunas, L.; Bachilo, S. M.; Fleming, G. R. *J. Phys. Chem. B* **2005**, *109*, 15671.
(16) Ma, Y. Z.; Valkunas, L.; Dexheimer, S. L.; Bachilo, S. M.; Fleming, G. R. *Phys. Rev. Lett.* **2005**, *94*, 157402.
(17) Ostojic, G. N.; Zaric, S.; Kono, J.; Strano, M. S.; Moore, V. C.; Hauge, R. H.; Smalley, R. E. *Phys. Rev. Lett.* **2004**, *92*, 117402.
(18) Huang, L. B.; Pedrosa, H. N.; Krauss, T. D. *Phys. Rev. Lett.* **2004**, *93*, 017403.
(19) Jones, M.; Engtrakul, C.; Metzger, W. K.; Ellingson, R. J.; Nozik, A. J.; Heben, M. J.; Rumbles, G. *Phys. Rev. B* **2005**, *71*, 115426.
(20) Sheng, C. X.; Vardeny, Z. V.; Dalton, A. B.; Baughman, R. H. *Phys. Rev. B* **2005**, *71*, 125427.
(21) Perebeinos, V.; Tersoff, J.; Avouris, P. *Nano Lett.* **2005**, *5*, 2495.
(22) Hagen, A.; Steiner, M.; Raschke, M. B.; Lienau, C.; Hertel, T.; Qian, H. H.; Meixner, A. J.; Hartschuh, A. *Phys. Rev. Lett.* **2005**, *95*, 197401.
(23) McDonald, T. J.; Jones, M.; Engtrakul, C.; Ellingson, R. J.; Rumbles, G.; Heben, M. J. *Rev. Sci. Instrum.* **2006**, *77*, 053104.
(24) Weisman, R. B.; Bachilo, S. M. *Nano Lett.* **2003**, *3*, 1235.
(25) O'Connor, D. V.; Phillips, D. *Time-Correlated Single Photon Counting*; Academic Press: Orlando, FL, 1984; p 288.
(26) Penzkofer, A.; Lammel, O.; Tsuboi, T. *Opt. Commun.* **2002**, *214*, 305.
(27) Chowdhury, F. N.; Kolber, Z. S.; Barkley, M. D. *Rev. Sci. Instrum.* **1991**, *62*, 47.
(28) Lefebvre, J.; Austing, D. G.; Bond, J.; Finnie, P. *Nano Lett.* **2006**, *6*, 1603.

NL0622808